Molecular and Brownian dynamics study of ion selectivity and conductivity in the potassium channel

T.W. Allen [a], M. Hoyles [a,b], S. Kuyucak [b], S.H. Chung [a,*]

[a] *Protein Dynamics Unit, Department of Chemistry, Australian National University, Canberra, ACT 0200, Australia*
[b] *Department of Theoretical Physics, Research School of Physical Sciences, Australian National University, Canberra, ACT 0200, Australia*

Received 8 July 1999; in final form 24 August 1999

Abstract

We employ recently revealed structural information for the potassium channel in molecular and Brownian dynamics simulations to investigate the physical mechanisms involved in the transport of ions across this channel. We show that ion selectivity arises from the ability of the channel protein to completely solvate potassium ions but not the smaller sodium ions. From energy and free energy perturbation profiles, we estimate the size of the energy barrier experienced by a sodium ion. Brownian dynamics simulations are carried out to determine conductance properties of this channel under various conditions. © 1999 Elsevier Science B.V. All rights reserved.

1. Introduction

Rapid growth in computer simulations in the last decade have provided many valuable insights into biological processes at the molecular level. Ion permeation in membrane channels is one such process where the only route from structure to function appears to be through large scale simulations. A great deal of progress has been made in understanding the ion transport across simpler channels (e.g., gramicidin), whose structures are well known [1]. Biological ion channels, on the other hand, are made of complex proteins [2], and progress has been hindered due to a lack of detailed structural knowledge. In a recent breakthrough, Doyle et al. determined the

crystal structure of the potassium channel from soil bacteria *Streptomyces lividans* [3], opening the way for detailed investigation of ion permeation through this channel via computer simulations.

Molecular dynamics (MD) simulations of ionic currents flowing across membrane channels is not yet within the reach of present supercomputers (a 4–5 order of magnitude increase in speed is required for that purpose). Nevertheless, one can use carefully tailored MD calculations to learn about specific features of a channel such as ion selectivity and diffusion, which in turn can be used in a simpler model that allows computation of current. In this letter we make use of the available structure of the K channel to examine solvation properties of K and Na ions, and compute energy and free energy perturbation profiles. The diffusion coefficient of K is also estimated in different regions of the channel. We then perform large time-scale Brownian dynamics (BD)

---

* Corresponding author. E-mail: shin-ho.chung@anu.edu.au; Fax: +61-6-247-2792.

simulations to study the conduction properties of the K channel.

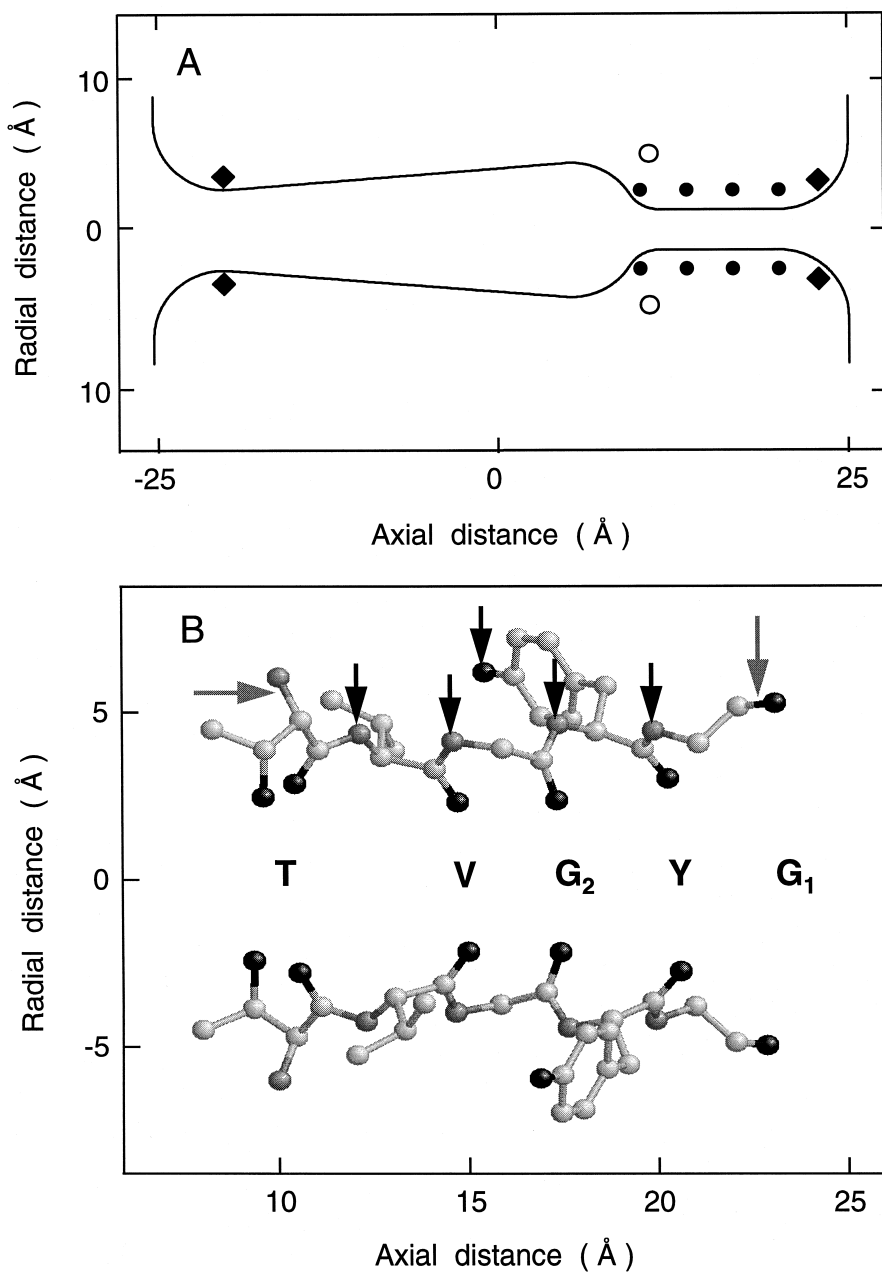Our model of the K channel is based on the protein structure detailed in Ref. [3]. The K channel

Fig. 1. (A) Cross section of the model channel. It extends from $z = -25$ Å to 25 Å with a narrow selectivity filter of radius 1.5 Å and length 12 Å. The poles of the helix dipoles are placed at $z = 10.66$ Å, $r = 5.66$ Å (open circles) and $z = 22$ Å, $r = 17$ Å, each pole carrying a charge of 0.6×10^{-19} C. Four mouth dipoles, each with a moment of 30×10^{-30} Cm, are placed at both entrances of the channel (diamonds). In BD simulations, carbonyl groups are represented by dipoles with moment 7.2×10^{-30} Cm, placed at $z = 10$, 13.33, 16.67 and 20.0 Å on the selectivity filter (filled circles). (B) Projections of two of the four peptide subunits forming the selectivity filter used in MD simulations. Carbon, nitrogen and oxygen atoms are shown in white, grey and black respectively.

is created by four subunits of a tetramer, each consisting of 158 KcsA signature sequence amino acids, of which 97 have been observed experimentally. An approximate trace of the pore size, taking account of atomic van der Waals radii, is illustrated in Fig. 1A. Here, we have used a slightly larger radius for the intracellular mouth, in line with the recent experiments which suggest that the crystal structure corresponds to the closed state and the mouth is larger in the open state [4]. The model channel has three distinct regions: a narrow selectivity filter near the extracellular reservoir, a large hydrophobic chamber and a long hydrophobic pore leading to the intracellular reservoir. With the exception of the selectivity filter region, the pore lining of the channel is formed mainly by hydrophobic residues that can be approximated by a one-dimensional Lennard–Jones (LJ) type function. The narrow selectivity filter region is, however, lined with carbonyl groups which are expected to play a pivotal role in ion discrimination. The 5 amino acid residues that make up the selectivity filter region are explicitly included in MD simulations (indicated by; T–threonine, V–valine, G–glycine and Y–tyrosine in Fig. 1B). These residues are attached to the remaining protein with harmonic constraints as shown by arrows in Fig. 1B (black–10 and gray–20 $kT/Å^2$). In BD simulations the polar carbonyl groups on these residues are represented by electric dipoles as shown in Fig. 1A. The electric dipoles associated with the pore helices and mouth dipoles performing the job of charged or highly polar groups near the channel entrances, are taken into account as shown in Fig. 1A. Reservoir regions are connected via a periodic boundary during all MD simulations.

2. Molecular dynamics simulations

MD simulations are performed using the CHARMM v25b2 code [5] with the CHARMM19 parameter set. We consider the ST2 [6], SPC/E [7] and TIP3P [8] water models for this study. The TIP3P model could not solvate the selectivity filter region, and therefore, it is excluded from further consideration. Our main simulations are performed with the ST2 model and comparisons are then made with the SPC/E model. Ion–ion potentials are taken from Ref. [9]. Ion–water potentials used with the ST2 model are from Ref. [9], while those used with the SPC/E model are from Ref. [10]. Ion–protein interactions are determined by standard combination rules involving the ion-ion and the CHARMM19 protein–protein potentials. The hydrophobic wall potential is represented by a Lennard–Jones (LJ) 5-3 potential which is derived by Boltzmann averaging the potential due to a regular array of 12–6 LJ centres on a cylinder [11]. A switched force cutoff for electrostatic interactions and a switched potential cutoff for LJ interactions are applied to groups at 12 Å.

A time step of 1 fs is used in the simulations with the Verlet MD algorithm. Velocity rescaling at 1 ps intervals leads to temperatures 300 ± 1 K. The 198 water molecules in the system are sampled from pre-equilibrated bulk coordinates at 1 g/cm^3. When the channel is immersed in water, in the absence of any external restraining potentials, the narrow segment of the selectivity filter widens. In order to hold the selectivity filter in place and mimic interactions with the remaining protein, weak harmonic constraints are applied at endpoints, sidechains and N–H bonds. As will be shown in a detailed study, provided the selectivity filter is supported by a minimal set of restraining potentials to prevent severe distortions, ion discrimination is fairly independent of the strength of these constraints [12]. In fact, discrimination appears to be a consequence of the equilibrium conformation of the protein. Bulk reference values for hydration and diffusion are derived from simulations of a periodic box of side 25.1 Å containing 525 ST2 water molecules and 1 ion. For the following discussion related to ion solvation, we note that the K ion first hydration radius and number are 2.82 ± 0.04 Å and 7.2 ± 0.1, while those for the Na ion are 2.34 ± 0.04 Å and 6.67 ± 0.02 respectively.

The carbonyl groups lining the selectivity filter play a key role in allowing one ionic species to traverse the channel, while rejecting another. Throughout the selectivity filter, the carbonyl oxygens provide almost a perfect match for the solvation of K^+, but are not as successful in coordinating a Na^+ ion. This point is illustrated in Fig. 2 where typical radial distribution functions of K^+ (A) and Na^+ ions (B) for both water and protein oxygen
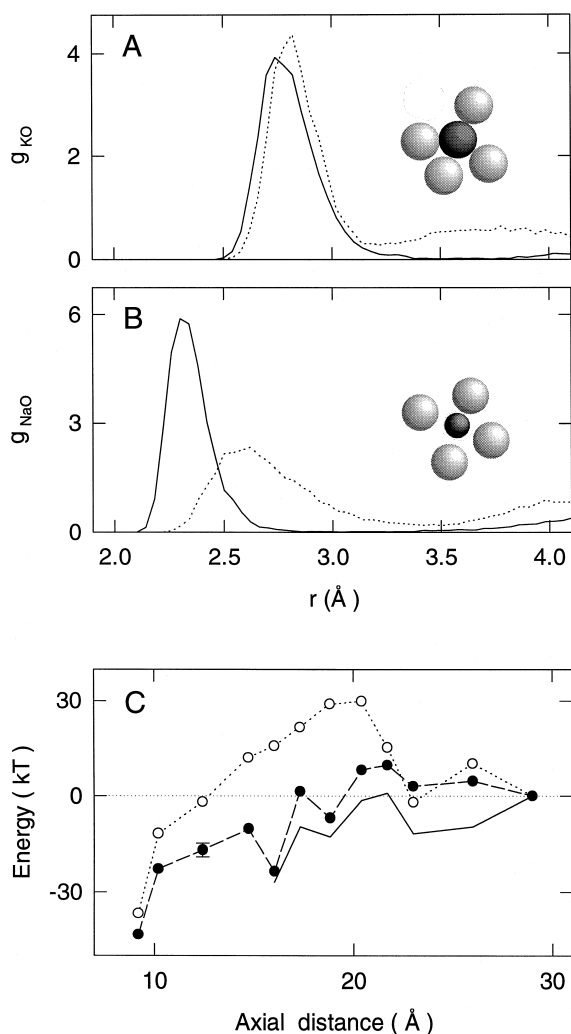
Fig. 2. (A) Radial distribution function g_{KO} for a K^+ ion held at $z = 14.7$ Å. The solid line shows g_{KO} for water oxygens and the broken line for protein oxygens. The inset shows an ion–carbonyl oxygen geometry representative of the simulation. (B) Same as A but for a Na^+ ion held at $z = 20.4$ Å. (C) The total energy of the system with respect to the upper reservoir is plotted against the ion position z for potassium (filled circles) and sodium (open circles). A profile for K^+ which includes the mouth dipoles is drawn as a solid line. During energy profile calculations an ion is held at a z value with a harmonic force (169 kT/Å^2). At least 500 ps of dynamics is carried out for each simulation.

atoms are plotted. As depicted in the inset, the large size of the K^+ ion (Pauling radius 1.33 Å) means that carbonyl oxygens sit well within the first hydration shell and this is evidenced by the overlapping

hydration and protein oxygen peaks in the radial distribution function. In contrast, the first protein oxygen peak in the radial distribution function of Na^+ (Pauling radius 0.95 Å) sits 0.28 ± 0.04 Å from the hydration peak. On average over the selectivity filter, there is a 0.34 ± 0.08 Å gap between the protein oxygen peaks and the bulk hydration peaks in the radial distribution functions for Na^+ compared with a 0.13 ± 0.02 Å average space for K^+.

The first coordination number for K^+ remains above the bulk hydration value throughout the selectivity filter, whereas there are regions where Na^+ is unable to meet this quota. The favorable interaction between K^+ and carbonyl oxygens, together with the helix dipoles, provides an attractive potential well. Sodium, on the other hand, is poorly solvated in regions where there is little stabilizing potential due to the helix dipoles and, as a consequence, experiences a significant energy barrier. The energy profile for K^+ is compared with that for Na^+ in Fig. 2C. It is clear that the channel will be impermeable to Na^+, as it experiences a steep energy barrier that reaches a maximum of 30 ± 4 kT. The smoothly falling barrier of Na^+ with pore helix field in comparison with the K^+ profile indicates the obvious involvement of the carbonyl oxygens in coordinating the K^+ ion as it traverses the selectivity filter. The remaining barrier at the channel entrance (10 ± 3 kT) is eliminated when mouth dipoles (representing charge moieties that are known to be present on the protein near the mouth region) are included, as indicated by the solid line in Fig. 2C.

To confirm that this high level of ion discrimination is not water model dependent we have repeated these simulations with the SPC/E model. This also enables us to carry out free energy perturbation calculations which are not possible with the ST2 model in CHARMM. Fig. 3A shows the total energy profiles of the K and Na which are qualitatively similar to those in Fig. 2C for the ST2 model. Although the ion discrimination is not as pronounced with the SPC/E water model (a consequence of a reduced hydration number for Na [11]), the function of the channel has not changed. The difference between the Na and K energies, with respect to the difference at the reservoir reference point ($z = 29$ Å) is plotted as a dotted curve in Fig. 3B. Using the PERT facility of CHARMM we have carried out free
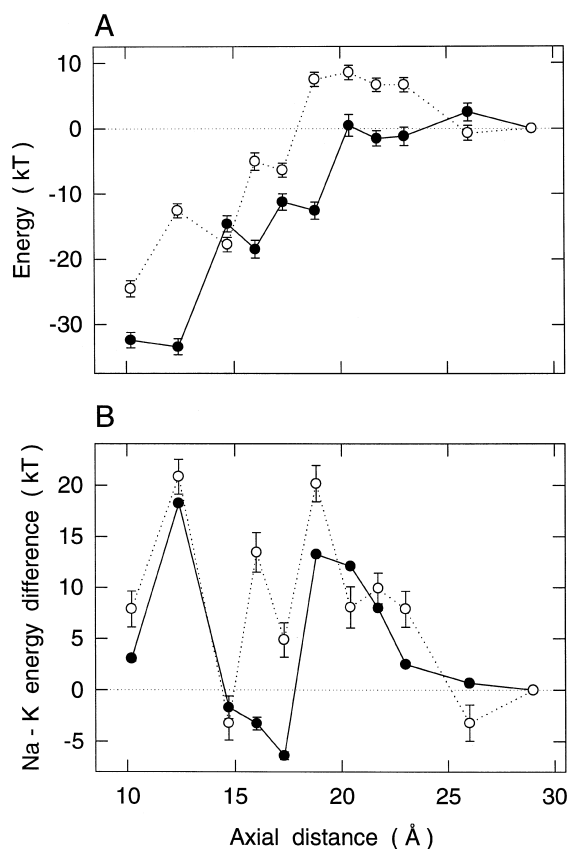
Fig. 3. Energy profiles with the SPC/E water model. (A) The total energy of the system with respect to the upper reservoir for K (filled circles) and Na (open circles) from 550 ps simulations. (B) The free energy difference associated with the transformation K → Na is plotted as a solid curve. Values are given with respect to the free energy difference at the reservoir reference point. Error bars are equal to the hysteresis from two opposite 120 ps simulations at each ion position. The dotted curve is the difference between Na and K total energies with respect to the reservoir.

energy perturbation calculations involving the transformation between K and Na ions. The free energy differences (again with respect to the reservoir value) are shown as a solid curve in Fig. 3B. It can be seen that the entropy components of the free energy alter relative barriers only very slightly throughout the majority of the filter region, with only the narrow central region near the V and G_2 residues ($z = 16$–17.3 Å) exhibiting sizable changes. The free energy perturbation analysis, therefore, reveals the same ion discrimination as the total energy analysis. The Na barriers, as much as 18 kT greater than those for the

K ion near the filter entrances, are certain to exclude this ion from the channel.

We complete this summary of MD findings with estimates of the axial ion diffusion for K, obtained by analysis of a suite of multiple ion configuration experiments totalling approximately 20 ns in simulation time. Our bulk reference value obtained with the ST2 model is 53% of the experimental value, as shown in Table 1. The axial ion diffusion coefficient averaged over the lower pore region ($-20 < z < 0$) is about half the bulk value, but it rises to the bulk levels in the wider chamber region ($0 < z < 10$). Such high levels of diffusion within hydrophobic pores have been observed also in studies of a model nAChR channel [15] and cylindrical channels [16]. Within the narrow selectivity filter ($10 < z < 20$) the mean diffusion coefficient drops to about $1/3$ of the bulk diffusion.

3. Brownian dynamics simulations

MD simulations can, in general, only be run for timescales of the order of 10 ns on a supercomputer, which is a small fraction of the time it takes for an ion to transit a channel. The alternative is to use a more phenomenological approach that is computationally less intensive. Here we use BD where only the motion of ions are followed via the Langevin equation

$$m_i \frac{d\mathbf{v}_i}{dt} = -m_i \gamma_i \mathbf{v}_i + \mathbf{F}_R + q_i \mathbf{E}_i. \tag{1}$$

The effect of the water molecules is represented in Eq. (1) by an average frictional force with a friction coefficient $m_i \gamma_i$, and a stochastic force $\mathbf{F}_R$ arising from random collisions. The last term in (1) is the total electric force acting on the ion due to other ions, fixed and induced surface charges in the protein, and the applied membrane potential. It is computed by solving Poisson's equation for a given channel boundary using an iterative numerical method as detailed elsewhere [18]. The Langevin Eq. (1) is solved at discrete time steps following the algorithm in Ref. [17].

We have previously used BD simulations to study the conductance properties of a number of model ion channels to which we refer for further technical details of the method [19–21]. Here we mention only

the novel aspects of the present BD simulations. An important parameter in the BD calculations is the effective dielectric constant of the channel, because it plays a critical role in determining the force acting on ions. MD simulations of water confined to small volumes suggest that ϵ is much reduced compared to the bulk value of 80 [22]. However what we are interested in here is the effective ϵ that reflects the capability of molecules surrounding an ion to solvate it and screen its charge. In this respect, our MD simulations (Fig. 2) indicate that this value could be fairly large for K ions. Since the value of ϵ in the channel is unknown, we use a range of values here and determine how the channel conductance depends on ϵ. For convenience the same value of ϵ is used in the channel and the reservoirs when solving Poisson's equation. The change in the Born energy is taken into account by including a smoothly varying potential step at either entrance of the channel. To simulate the effects of short range forces more accurately, the two time-step algorithm developed in Ref. [20] is employed. A shorter time step of 2 fs is used at the intracellular entrance and filter regions ($-25 < z < -15$ and $7.5 < z < 25$), and a long time step of 100 fs is used elsewhere. A second important input in BD calculations is the diffusion constant of ions. While the MD study in Table 1 indicates that ion diffusion rate could be reduced to as little as $1/3$ of the bulk value, such variations have led to relatively minor changes in the channel conductance in the BD studies [12]. Therefore the bulk values of the ion diffusion constants are used in the present BD simulations.

In order to get an intuitive feeling for the ensuing BD simulations, we first show the effect of various charge groups on the potential profile of a single ion in Fig. 4. In the absence of any fixed charges on the protein wall, an ion faces a large barrier of height 20
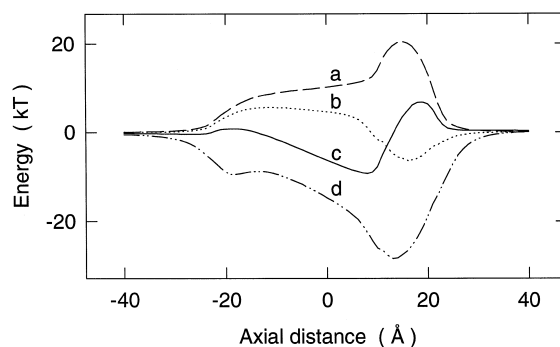

Fig. 4. Electrostatic energy profiles of a cation along the central axis of the channel when the effective dielectric constant of the channel is $\epsilon = 60$. The curves are explained in the text.

kT (profile **a**). Inclusion of either the dipoles in the selectivity filter (**b**) or the helix dipoles (**c**) transforms a section of the barrier into a well. When both sets of dipoles, as well as two rings of mouth dipoles, are included, the profile becomes a deep potential well of depth 30 kT (**d**). The depth of the well depends on the value of ϵ used, and it increases with decreasing ϵ. Electrostatic calculations show that this well is deep enough to hold two ions in a stable configuration. A third ion entering the channel sees a barrier arising from the combination of the channel potential and the Coulomb repulsion due to the first two ions. The height of this barrier V_B depends critically on the dielectric constant assumed for the channel: for $\epsilon = 20$, 40, 60, and 80, respectively, $V_B = 11.8$, 5.8, 3.6, and 2.2 kT. These results suggest that two K ions could be resident in the channel, and the effective dielectric constant needs to be fairly large for conduction to take place.

An extensive set of BD simulations are carried out to study the influence of the dipole moments and the dielectric constant on the channel conductance. The moments of the carbonyl dipoles are well established but those of the helix and mouth dipoles are not well known. When the helix dipole moments are increased, the conductance first increases, reaching a maximum value and then decreases. The mouth dipoles exhibit a similar behaviour. The same optimal dipole strengths (quoted in Fig. 1) are found for different values of ϵ, which we use in the rest of the BD simulations. The charge on the helix dipole (0.6×10^{-19} C) is close to a theoretically deduced value (0.8×10^{-19} C) [23]. A similar optimization

Table 1
Axial ion diffusion estimates for K in different regions of the channel (in units of $\text{Å}^2/\text{ps}$). Experimental and bulk values are also given for comparison

Exp [14].	0.196
Bulk	0.104 ± 0.007
$-20 < z < 0$	0.045 ± 0.008
$0 < z < 10$	0.10 ± 0.03
$10 < z < 20$	0.04 ± 0.03

for the carbonyl dipoles reproduces the known value $(7.2 \times 10^{-30}$ Cm$)$, which gives us confidence in the present BD simulations. The effect of reducing ϵ from 80 is to suppress the conductance progressively until $\epsilon = 40$, below which no conduction takes place. The physiological conductance of approximately 40 pS [24] is obtained when $\epsilon = 60$. Higher levels of conductances have been observed in some experiments when pH levels are lowered [25]. This may be due to protonation of the fixed charges in the channel.

In the remaining part, we deduce some of the salient characteristics of the channel under the assumption that $\epsilon = 60$. The current–voltage relationship, shown in Fig. 5A, is obtained with symmetrical solutions of 300 mM in both reservoirs (the height of the reservoirs is adjusted to 27 Å). The *I–V* curve is asymmetric and deviates systematically from Ohm's law for $|V| > 100$ mV. These features follow from the presence of energy barriers in the channel. Intuitively, a barrier is less of an impediment to an ion when the driving force is large. Thus, in the presence of barriers, Ohm's law is modified by a function of the form [20,21]

$$I = \frac{\gamma V}{1 + \beta / \left[\exp(eV/V_{B1}) + \exp(-eV/V_{B2}) \right]}$$

$$(2)$$

where γ is the limiting conductance, β is a dimensionless parameter and V_{Bi}, are the effective barriers seen by ions moving inward $(i = 2)$ or outward $(i = 1)$. The well known rectification property [2] arises from the fact that ions moving into and out of the cell see different barriers. When $eV \gg V_{Bi}$, the denominator in Eq. (2) goes to 1, and one recovers Ohm's law. For $eV \ll V_{Bi}$, the relationship is again linear but with the conductance reduced to $\gamma/(1 + \beta/2)$. In the curve fitted through the data points (Fig. 5A), the transition between these two limits takes place around $V = 100$ mV. When the solutions in the two reservoirs have different concentrations, the asymmetry between the inward and outward currents is accentuated, and the simulation results can be fitted with Eq. (2) multiplied by the Goldman factor, which is traditionally used in describing channel currents due to asymmetric concentrations [2]. Our simulation results thus suggest that careful de-
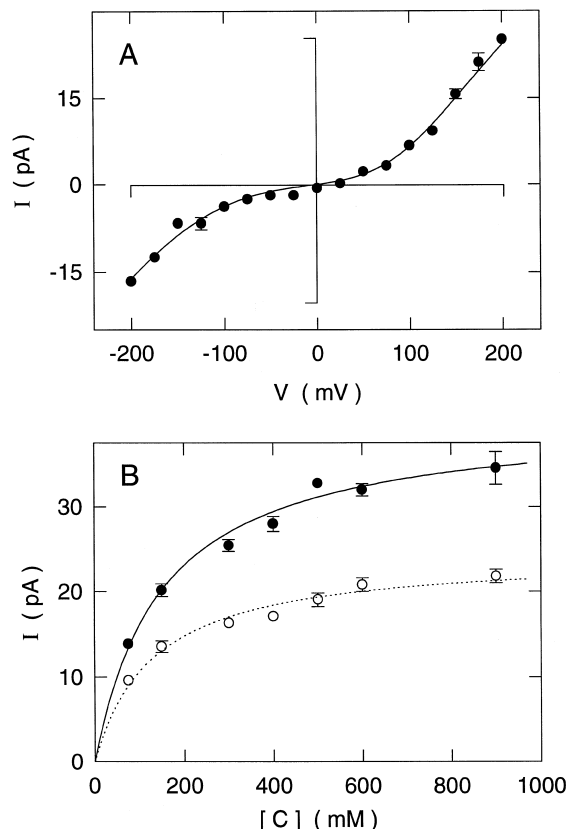

Fig. 5. (A) The *I–V* curve for symmetrical solutions. Simulations with 13 K and 13 Cl ions in each reservoir, lasting 100 ns, are repeated for 5 times. The solid line is calculated from Eq. (2) with $\gamma = 133 \pm 15$ pS, $\beta = 10 \pm 4$, $V_{B1} = 1.7 \pm 0.4$ kT and $V_{B2} = 2.9 \pm 0.7$ kT. (B) The conductance–concentration curves obtained with symmetrical solutions, and an applied potential of $+200$ mV (filled circles) and -200 mV (open circles). The lines are fits to the Michaelis–Menten equation with $I_{max} = 41 \pm 1$ pA and $K_s = 151 \pm 11$ mM (filled circles), $I_{max} = 24.2 \pm 0.8$ pA and $K_s = 127 \pm 11$ mM. (open circles)

termination of the current–voltage relationships in a range that goes beyond the usual measurements (e.g., ± 250 mV) could yield useful information about the permeation mechanisms in real biological channels.

In Fig. 5B we show the concentration dependence of the current, which exhibits the same saturation property as observed experimentally [26]. Saturation of current is expected to occur when the transport of ions across the channel is determined by two independent processes, one of which depends upon the concentration and one that does not [20]. Under this condition, the conductance–concentration curve is

given by the Michaelis–Menten equation, $I = I_{max}/(1 + K_s/[c])$, that describes the saturation of current with concentration $[c]$ [2].

4. Conclusions

In conclusion, we have used the recently unveiled structural information about the potassium channel in molecular and Brownian dynamics studies to understand its selectivity and conduction properties. The selectivity property is shown to arise from almost perfect solvation of K ions in the filter region. The smaller Na ions are not as well solvated leading to a relatively large energy barrier for them to enter the channel. Ion diffusion estimates from these MD simulations show considerable attenuation near the narrow channel entrance regions. BD simulations with variable diffusion coefficients in the selectivity filter region have demonstrated that large channel conductance can emerge, despite this reduced ion mobility. In the BD simulations, we have found that for the channel to conduct and reproduce the experimentally observed properties, a fairly large value of the dielectric constant is required ($\epsilon > 40$). Understanding this feature of the K channel will be one of the challenges for the future MD studies.

The K channel is known to be a multi-ion channel. Therefore, it is of interest to comment on the average number and positions of K ions in the channel. In the BD simulations, in agreement with the intuitive expectations from the electrostatic calculations, the average number is found to be 2. These ions most commonly dwell near the equilibrium positions of two ions in the potential well (**d**) in Fig. 4. MD studies are found to support this picture of the K channel with two ions resident in the channel on average. Details of the present work will be published in forthcoming articles [12,13]. MD simulations, where the whole channel structure is implemented, is in progress and will provide a test for the assumptions made in this article when finished.

Acknowledgements

References

[1] B. Roux, M. Karplus, Annu. Rev. Biophys. Biomol. Struc. 23 (1994) 731.
[2] B. Hille, Ionic Channels of Excitable Membranes, Sinauer Associates Inc., Sunderland, MA, 1992, 2nd ed.
[3] D.A. Doyle, J.M. Cabral, R.M. Pfuetzner, A. Kuo, J.M. Gulbis, S.L. Cohen, B.T. Chait, R. MacKinnon, Science 280 (1998) 69.
[4] E. Perozo, D.M. Cortes, L.G. Cuello, Nature Struct. Biol. 5 (1998) 459; Science 285 (1999) 73.
[5] B.R. Brooks, R.E. Bruccoleri, B.D. Olafson, D.J. States, S. Swaminathan, M. Karplus, J. Comput. Chem. 4 (1983) 187.
[6] F.H. Stillinger, A. Rahman, J. Chem. Phys. 60 (1974) 1545.
[7] H.J.C. Berendsen, J.R. Grigera, T.P. Straatsma, J. Phys. Chem. 91 (1987) 6269.
[8] W.L. Jorgensen, J. Chandrasekhar, J.D. Madura, R.W. Impey, M.L. Klein, J. Chem. Phys. 79 (1983) 926.
[9] K. Heinzinger, Physica B 131 (1985) 196.
[10] B.M. Pettit, P.J. Rossky, J. Chem. Phys. 84 (1986) 5836.
[11] T.W. Allen, S. Kuyucak, S.H. Chung, J. Chem. Phys., 1999, in press.
[12] T.W. Allen, S. Kuyucak, S.H. Chung, to be published in Biophys. J.
[13] S.H. Chung, T.W. Allen, M. Hoyles, S. Kuyucak to be published in Biophys. J.
[14] D.R. Lide, editor, CRC Handbook of Chemistry and Physics, CRC Press, Cleveland, 1994.
[15] G.R. Smith, M.S.P. Sansom, Biophys. J. 75 (1998) 2767.
[16] R.M. Lynden-Bell, J.C. Rasaiah, J. Chem. Phys. 105 (1996) 9266.
[17] W.F. van Gunsteren, H.J.C. Berendsen, Mol. Phys. 45 (1982) 637.
[18] M. Hoyles, S. Kuyucak, S.H. Chung, Biophys. J. 70 (1996) 1628; Comput. Phys. Commun. 115 (1998) 45.
[19] S.C. Li, M. Hoyles, S. Kuyucak, S.H. Chung, Biophys. J. 74 (1998) 37.
[20] S.H. Chung, M. Hoyles, T.W. Allen, S. Kuyucak, Biophys. J. 75 (1998) 793.
[21] M. Hoyles, S. Kuyucak, S.H. Chung, Phys. Rev. E 58 (1998) 3654.
[22] L. Zhang, H.T. Davis, D.M. Kroll, H.S. White, J. Chem. Phys. 99 (1995) 2878, and references therein.
[23] W.G.H. Hol, P.T. van Duijnen, H.J.C. Berendsen, Nature 273 (1978) 443.
[24] H. Schrempf et al., EMBO J. 14 (1995) 5170.
[25] L.G. Cuello, J.G. Romero, D.M. Cortes, E. Perozo, Biochemistry 37 (1998) 3229.
[26] R. Coronado, R.L. Rosenberg, C. Miller, J. Gen. Physiol. 76 (1980) 425.